Article

Sound-Quality-Based Decision Making in Multiobjective Optimisation of Operations for Sustainable Airport Scenarios

Umberto Iemma * and **Francesco Centracchio**

Department of Engineering, Roma Tre University, Via Vito Volterra, 62, 00146 Roma, Italy;
francesco.centracchio@uniroma3.it
* Correspondence: umberto.iemma@uniroma3.it

Abstract: The paper deals with a community-oriented approach to the multiobjective optimisation of sustainable takeoff and landing procedures of commercial aircraft. The objective functions to be minimised are defined as the measure of area surrounding the airport where the Sound Exposure Level (SEL) is higher than 60 dBA, and the amount of fuel burned during the procedure. The first merit factor is a measure of the number of citizens affected by a potentially harmful noise level, whereas the second is proportional to the chemical emissions. The novelty of the present approach is the use of a criterion based on sound quality for the selection of the optimal procedure from the Pareto front set. The spectrum of the noise produced by each non-dominated solution is compared to a reference spectrum, the target sound. This is synthesised to meet the acceptance requirements that emerged by a campaign of psychometric tests. The rationale underlying the research is tightly linked to the expected transformation of civil aviation, with the advent of new air transport solutions in urban and suburban environments. The breakthrough nature of the emerging scenarios requires a drastic renewal of the approaches used in the management of operations, and the present work represents a contribution to this evolution. The optimisation is attained adopting a global, deterministic method, and numerical results are obtained for single- and twin-aisle aircraft.

Keywords: multiobjective optimisation; community noise; air quality; sound quality; noise abatement procedures; spectral matching

1. Introduction

The evolution of the air transportation system is nowadays experiencing a turning point that will lead to the advent of a completely new scenario in the next decade. Electrification of propulsion, Urban Air Mobility (UAM), suburban air shuttles, and alternative fuels are some of the factors that are inducing a change of paradigm for civil aviation. The effect on society of these ground-breaking solutions is amplified by the enduring expansion of urban areas around airports and the constant increase in air traffic in terms of daily movements and passengers (for additional information and details see Knobloch et al. [1]). In such a rapidly evolving context, sustainability can be guaranteed only introducing new approaches to the management of the air transportation system, capable of satisfying market requests and, at the same time, preserving the health and the quality of life of citizens. The European community has sponsored several research projects over the last twenty years to develop disruptive technologies and operational procedures to lower the impact on the community of the chemical and acoustic emissions related to civil aviation.

A standard trajectory optimisation is aimed at calculating the best flight path through the minimisation (or maximisation) of a performance index that can deal with noise reduction (in a specific point or in a certain area), fuel consumption or the total cost [2]. The growth of computational resources, together with the development of sophisticated multiobjective optimisation algorithms have made it possible to deal with the design of the trajectories as a vector minimisation problem (a valuable review of Multi-Objective

Trajectory Optimisation techniques for transport aircraft flight operations can be fund in Gardi et al. [3]), so that multiple environmental factors can be minimised at the same time [4]. When the main focus is on noise reduction, the resulting flight path can be named a noise abatement procedure (NAP). NAPs can involve, in order to avoid overflight of populated areas, preferential routings [5] to cope with the well-being of populations living near airports. The NAP design for airport noise mitigation is usually carried out by airlines [6] under the guidance of the International Civil Aviation Organization (ICAO) and regulatory entities such as the Federal Aviation Administration (FAA). Notwithstanding, over the past decades, universities and research centres have also been involved in the design of environmentally friendly airport procedures: indeed, this activity provides the possibility of developing sophisticated flight simulation tools involving flight dynamics and control, multilevel computational aeroacoustics techniques together with numerical optimisation strategies [7–11]. To date, one of the most challenging research topics related to the design of low environmental impact trajectories is the adaptation of the NAP design techniques to the new aircraft concepts, such as the Blended Wing Body (BWB) configuration: for such disruptive layouts the designer cannot rely on past experience; thus, a viable strategy appears to be metamodelling the BWB shielding effect [12,13], with the aim of exploiting the existing well-assessed noise estimation tools for the prediction of future airport scenarios.

The work presented in this paper is different from traditional trajectory optimisations, and it can be considered as an evolution of the approach first introduced during the SEFA projects (Sound Engineering For Aircraft, FP6, 2004–2007 [14–16]) to assess the perceptive qualities of the noise produced by a civil aircraft, and subsequently evolved to an airport scenario (i.e., a prescribed sequence of takeoff and landing procedures) during COSMA (community noise solutions to minimise aircraft noise annoyance, FP7, 2009–2012 [17,18]). Here, the sound quality assessment is applied in the multiobjective context adopted in the ANIMA project (Aviation Noise Impact Management through Novel Approaches, H2020, 2017–2021, [1,19]) as a criterion to select the least annoying procedure from the Pareto set of a two-objective optimisation. The objective functions used are indirect measures of the number of citizens affected by a potentially harmful noise level, and of the amount of greenhouse gases injected in the atmosphere.

Specifically, this work aims at exploring multiple noise descriptors for the design of low-noise flight paths. Indeed, the purpose of the analysis presented here is to simultaneously minimise both the chemical and the acoustic emissions: the case studies concern the takeoff and the approach procedures of single- and twin-aisle aircraft, representative of aeroplane classes used for most of the international commercial routes. Since the Multi Objective Optimisation (MOP) solution is composed of a set of non-dominated points, the sound quality assessment is applied to select the optimal trajectories. The aircraft operations have been optimised within the in-house Multidisciplinary Conceptual Robust Design Optimisation (MCRDO) framework FRIDA (Framework for Innovative Design in Aeronautics [12,15,16,18,20–22]). The two objectives to be minimised are the Sound Exposure Level (SEL) 60 dBA contour area and the amount of fuel burnt during the entire airport operation. The decision making criterion makes use of a third objective function, built based on the sound-quality assessment: the latter is formalised as the L^p norm in the vector space defined by the difference between the noise produced by the aircraft and a weakly annoying target sound (the interested reader can find useful information on the target sound definition in [18]). It is worth highlighting that L^p norms of different orders can be used to build objectives that focus on local and distributed differences: this behaviour has been investigated concerning benchmark problems [16], and it can be demonstrated that it can be exploited when the effect of tonal components is explicitly available. The constrained optimisation problem is solved within FRIDA by using the Deterministic Particle Swarm Optimisation (DPSO) method, a gradient-free global technique introduced by Kennedy and Russel [23], in its original deterministic implementation [24,25]. All the numerical results are presented in terms of approximated Pareto frontiers for takeoff and landing conditions for both the single- and twin-aisle aircraft.

The paper is organised as follows. Section 2 provides details on the optimisation problem setup, including the definition of the two objectives functions. The main characteristics of both the single- and twin-aisle aircraft are reported in Section 3. In Section 4, the optimisation results are presented, and the criteria for the sound-quality-based decision making are reported in Section 5 with the final designer choices. Finally, Section 6 presents some concluding remarks.

2. Optimisation Problem Setup

A Generic Constrained Multiobjective Optimisation Problem (MOP) is formalised as

$$
\begin{aligned}
\min/\max[J_k(\mathbf{x})], \quad & k = 1, \ldots, K \text{ and } \mathbf{x} \in \mathcal{D} \\
\text{with bounds } x_n^L \leq x_n \leq x_n^U, \quad & n = 1, \ldots, N \\
\text{subject to } g_i(\mathbf{x}) \leq 0, \quad & i = 1, \ldots, I \\
\text{and } h_j(\mathbf{x}) = 0, \quad & j = 1, \ldots, J
\end{aligned}
\tag{1}
$$

where $J_k(\mathbf{x})$ is the k-th objective function (with $\mathbf{x} \in \mathcal{D}$ being the vector containing the N design variables), and $g_i(\mathbf{x})$ and $h_j(\mathbf{x})$ are the inequality constraints and the equality constraints, respectively. The solution of the above problem consists of the set of non-dominated solutions that forms the Pareto frontier.

In the present multiobjective approach, the two merit functions are related to acoustic and chemical emissions. The acoustic descriptor used here is the Sound Exposure Level (SEL) which represents the most suitable strategy for comparing airport procedures of different durations. Here, the objective function to be minimised is chosen to be a measure of the number of citizens affected by a noise level above a certain threshold. More specifically, $J_1(\mathbf{x})$ is chosen as the area bounded by the SEL 60 dBA contour, formalised as

$$
J_1(\mathbf{x}) = \iint_{A_{60}} dA \quad \{A_{60} : \forall (\xi, \eta) \in A_{60} \Rightarrow \text{SEL}(\mathbf{x}, \xi, \eta) \geq 60 \text{ dBA}\}
\tag{2}
$$

where A_{60} is the area surrounding the airport where SEL is greater or equal to 60 dBA, with ξ and η being the reference spatial coordinates of the noise map. The objective function related to the chemical emission is simply the amount of fuel burnt during the manoeuvre,

$$
J_2(\mathbf{x}) = \int_0^{t_{10k}} cT dt
\tag{3}
$$

where t_{10k} is the time that the aircraft takes to reach an altitude of 10,000 ft, T is the required thrust and c is the specific fuel consumption, here modelled as a function of the true air speed (TAS).

With the aim of ensuring the simulation of a realistic operation, suitable constraints were imposed. First of all, the high-lift devices deployment combined with the angle of attack must ensure a vertical equilibrium, preventing the stall at the p-th trajectory sample. Thus, the following constraint is imposed

$$
g_1(\mathbf{x}) = \sum_{p=1}^{P} \max\left(0, \frac{\alpha_p}{\alpha_{ST}} - 1\right)
\tag{4}
$$

where α_{ST} is the stall angle. Furthermore, since N1 (the rotational velocity of the low-pressure spool) must not exceed the overspeed in takeoff and must not fall below the idle setting in the approach (T and A indicate the takeoff and the approach procedures), the following constraints are also used

$$g_2(\mathbf{x})|_T = \sum_{p=1}^{P} \max\left(0, \frac{N1_p}{N1_{OS}} - 1\right)$$

$$g_2(\mathbf{x})|_A = \sum_{p=1}^{P} \max\left(0, 1 - \frac{N1_p}{N1_{ID}}\right)$$

(5)

where the subscripts *OS* and *ID* stand for overspeed and idle, respectively. To avoid structural failures, the following constraints, which account for the normal load factor *n* variation, are imposed

$$g_3(\mathbf{x}) = \sum_{p=1}^{P} \max\left(0, \frac{n_p}{n_L^+} - 1\right)$$

(6)

$$g_4(\mathbf{x}) = \sum_{p=1}^{P} \max\left(0, 1 - \frac{n_p}{n_L^-}\right)$$

(7)

where n_L^+ and n_L^- are the positive and negative limit normal load factor. Equations (4)–(7) are calculated at each *p*-th sample of the trajectory. In addition, considering the *q*-th trajectory segment the following constraint was introduced

$$g_5(\mathbf{x}) = \sum_{q=1}^{Q} \max\left(0, \frac{|\gamma_q|}{\gamma_{MAX}} - 1\right)$$

(8)

to account for the maximum absolute value of the ramp angle over the *Q* trajectory segments. Finally, the maximum change in slope $\Delta\gamma_{MAX}$ between two consecutive trajectory segments was imposed as

$$g_6(\mathbf{x}) = \sum_{q=1}^{Q} \max\left(0, \frac{|\gamma_q - \gamma_{n-1}|}{\Delta\gamma_{MAX}} - 1\right)$$

(9)

where $2 < q < Q$, to ensure passenger comfort.

It is important to underline that the correct estimation of $J_1(\mathbf{x})$ requires the use of suitable aeroacoustic models: indeed, the prediction of the noise at a prescribed location requires both the modelling of the relevant physical phenomena involved in the sound generation and propagation mechanisms. Within the optimisation context, the identification of a proper trade-off between accuracy and computational cost is a crucial aspect: thus, well-assessed semi-empirical models were used here, capable of predicting the aircraft noise spectra at specified location (for useful details, see Appendix A). In addition, it is worth noting that the deep interplay between aeroacoustics and flight mechanics makes a correct description of the aircraft dynamics and its operating conditions mandatory. Specifically:

- The airframe noise during the airport operations is also linked to the deployment of the high lift devices;
- Due to the strong directivity of some acoustic sources, the attitude of the aircraft influences the spectrum that reaches a listener;
- The noise emitted by the main sources related to the propulsion system (fan, compressor, turbine, buzz-saw and jet) depends on the engine's settings in terms of N1 and N2, which depends on the required thrust;
- The relative speed and the distance between the aircraft and the listener influence the spectrum of the received signal through the Doppler effect and the atmospheric absorption.

Therefore, a detailed description of the aircraft flight mechanics makes it possible to provide an adequate estimate of the noise emissions. Interestingly, since $J_2(\mathbf{x})$ also depends on the required thrust, the two objective functions are intrinsically connected.

3. Case Studies

The case studies involve both a single- and a twin-aisle aircraft, representative of aeroplane classes used for most of the international commercial routes: the first one for short- and medium-haul flights, and the second for medium- to long-haul ones. The aircraft characteristics are reported in Table 1.

Table 1. Main characteristics of the single- and twin-aisle aircraft.

A/C Charachteristics	Single-Aisle	Twin-Aisle
Number of seats	164	406
Cruise Mach number	0.78	0.82
Cruise altitude (ft)	42,000	42,000
Range (nmi)	3250	5500
MTOW (ton)	78	230
OEW (ton)	43	122
Number of engines	2	2
Maximum thrust per engine (kN)	111.2	316.4
Bypass ratio	6.5	9.6
Engine placement	under the wing	under the wing

The framework FRIDA builds the aircraft geometrical model, performing a complete analysis for the estimate of aerodynamic and the structural properties. In Figure 1 are presented the pictorial representations of the models built within FRIDA related to the single- and the twin-aisle aircraft.
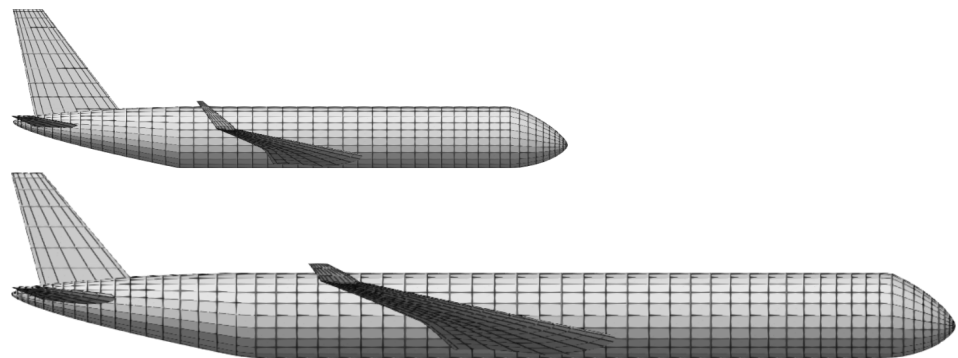
Figure 1. Side view of the geometrical models generated by FRIDA for the single- (**top**) and the twin-aisle (**bottom**) aircraft.

All the data coming from the analysis modules are collected and passed to the FRIDA flight simulation environment. With the aim of reducing the computational effort, suitable corrections are applied to the aerodynamic and inertial data to account for the specific flight conditions: by doing this, the airport manoeuvres can be calculated with the expense of a single aircraft analysis, maintaining an accuracy more than acceptable.

In this work, both takeoff and landing procedures are optimised. Specifically, the reference takeoff manoeuvres are modelled starting from the ICAO procedures for aircraft compatible with the test cases analysed. The trajectories consist of five segments (six input nodes), starting from the brake release up to a distance related to an altitude equal to 10.000 ft (about 35 km from the runway for both the aircraft). The trajectory description is built starting from nodal variables (geometric and kinematic), reported in Table 2.

Table 2. Reference takeoff manoeuvre for the single- and twin-aisle aircraft: geometric and kinematic variables.

Op. #	Single-Aisle			Twin-Aisle		
	x (m)	z (m)	v (m/s)	x (m)	z (m)	v (m/s)
1	0.0	0.0	0.0	0.0	0.0	0.0
2	1698.6	0.0	83.7	1908.1	0.0	87.9
3	4500.4	457.2	85.6	4772.2	457.2	89.9
4	8648.7	914.4	87.5	9571.5	914.4	91.9
5	15,852.8	1179.4	136.2	16,285.3	1132.4	135.9
6	35,441.3	3048.0	149.7	35,833.9	3048.0	149.7

The initial aircraft masses for the takeoff phase were set approximately equal to 77 tons for the single-aisle aircraft and 217 tons for the twin-aisle, corresponding to 98% and 95% of the MTOW, respectively. In Figure 2 are depicted the reference takeoff trajectories for the single- and the twin-aisle aircraft with the 60 dBA isolevel.

(**a**)

(**b**)
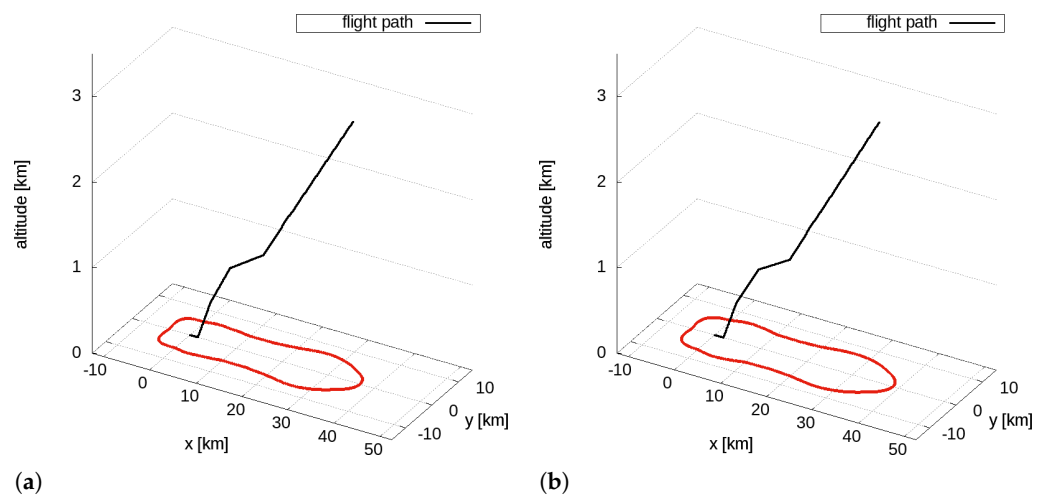
Figure 2. Flight path and 60 dBA isolevel for the reference takeoff manoeuvre. (**a**) single–aisle aircraft and (**b**) twin–aisle aircraft.

The reference approach phases are modelled based on the standard ICAO procedures for two aircrafts compatible with the test cases chosen. The trajectory consists of six segments (seven input nodes), starting at about 40 km from the airport and ending at the touchdown point on the runway. The geometric and the kinematic variables of the nodes are reported in Table 3.

Table 3. Reference approach manoeuvre for the single- and twin-aisle aircraft: geometric and kinematic variables.

Op. #	Single-Aisle			Twin-Aisle		
	x (m)	z (m)	v (m/s)	x (m)	z (m)	v (m/s)
1	−39,213.1	1828.8	140.6	−43,346.7	1828.8	140.6
2	−24,262.8	914.4	134.4	−26,462.8	914.4	134.4
3	−17,447.8	914.4	98.0	−17,447.8	914.4	89.3
4	−15,202.8	796.7	92.9	−14,813.2	776.3	82.3
5	−10,297.6	539.7	70.0	−12,164.6	637.5	69.4
6	0.0	0.0	68.2	0.0	0.0	68.4
7	925.1	0.0	15.4	641.4	0.0	15.4

The initial masses for the approach phase for the single- and twin-aisle aircraft are about 58 tons and 157 tons, respectively, corresponding to 135% of the OEW for the single-

aisle aircraft and 129% of the OEW for the twin-aisle. The reference approach trajectories for the single- and the twin-aisle aircraft with the 60 dBA isolevel are depicted in Figure 3.

(**a**) (**b**)
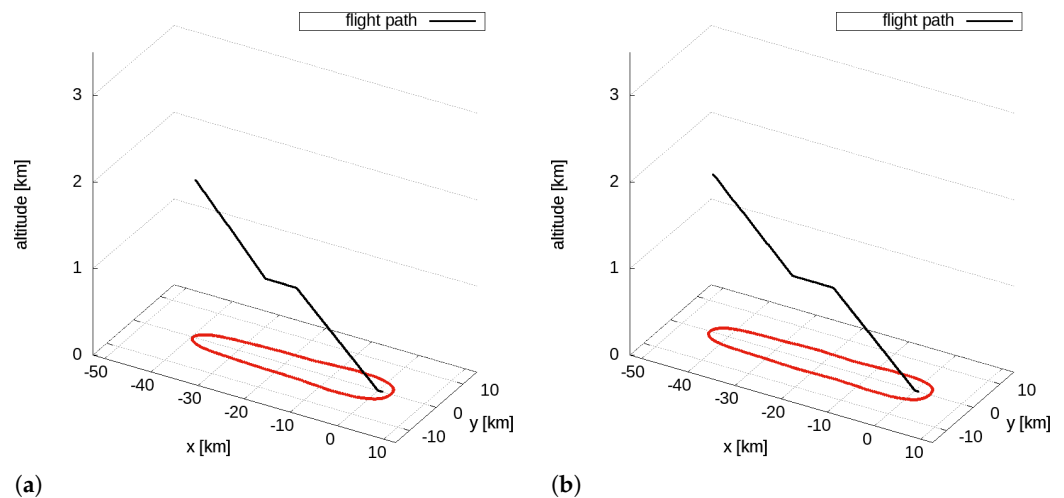
Figure 3. Flight path and 60 dBA isolevel for the reference approach manoeuvre. (**a**) single–aisle aircraft and (**b**) twin–aisle aircraft.

4. Optimisation Results and Discussion

The optimisations were carried out within FRIDA, using the Deterministic Particle Swarm Optimisation (DPSO) algorithm, an original implementation of the Particle Swarm Optimisation (PSO) method, making use of $10n_{DV}$ particles (with n_{DV} being the number of design variables) and 250 PSO iterations. Instead of solving an unconstrained minimisation problem, pseudo-objective functions are used to account for the constraints described by Equations (4)–(9): the pseudo-objective $\hat{J}_k$ is defined using the external quadratic penalty function as follows

$$\hat{J}_k(\mathbf{x}) = J_k(\mathbf{x}) + \frac{1}{\varepsilon} \sum_i \max[0, g_i(\mathbf{x})]^2 \tag{10}$$

where ε is the penalty coefficient. The optimisation process for the takeoff is aimed at finding the optimal path in terms of spatial and kinematic variables of the third, the fourth and the fifth trajectory nodes, whereas the landing optimisation involves the second, the third and the fourth trajectory nodes (see Tables 2 and 3). The results are reported below in terms of DPSO solutions with the approximated Pareto frontiers: for both the single- and the twin-aisle aircraft under consideration, the optimal solutions related to the minimum noise and the minimum fuel are presented and discussed.
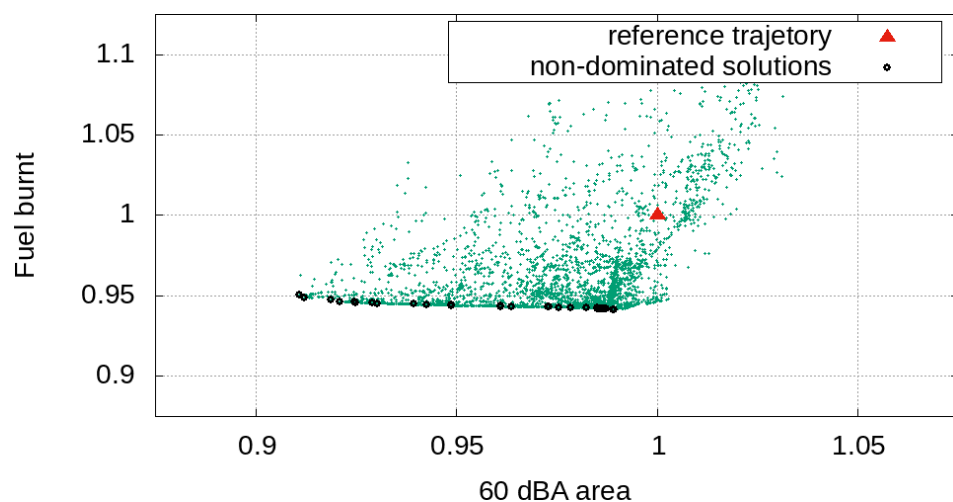
4.1. Single-Aisle Aircraft
4.1.1. Takeoff

The optimisation process for the takeoff is aimed at finding the optimal path in terms of spatial and kinematic variables of three nodes (the third, the fourth and the fifth trajectory node). The design variables with the upper and lower bounds are reported in Table 4.

Figure 4 shows the optimisation results for the single-aisle aircraft takeoff operation in terms of DPSO solutions (normalised with respect to the reference solution) and the approximated Pareto front.

Table 4. Takeoff manoeuvre optimisation variables for the single-aisle aircraft: reference values with upper and lower bounds.

Variable	Lower Bound	Reference	Upper Bound
x_3 (m)	4000.0	4500.4	5000.0
z_3 (m)	400.0	457.2	500.0
v_3 (m/s)	85.0	85.6	86.0
x_4 (m)	7000.0	8648.7	10,000.0
z_4 (m)	800.0	914.4	1000.0
v_4 (m/s)	87.5	87.5	110.0
x_5 (m)	13,000.0	15,852.8	17,000.0
z_5 (m)	1000.0	1179.4	1300.0
v_5 (m/s)	110.0	136.2	140.0

Figure 4. Takeoff manoeuvre for the single-aisle aircraft: normalised DPSO solutions with reference trajectory and approximated Pareto front.

The analysis of the non-dominated solutions in Figure 4 highlights that there is the possibility of decreasing the 60 dBA area by about 9% starting from the minimum fuel solution moving along the Pareto front. In addition, it is worth noting that the entire approximated Pareto frontier is composed of solutions that improve both the acoustical and chemical emissions with respect to the reference takeoff trajectory. The optimal solutions related to the minimum noise and the minimum fuel consumption are presented in Figure 5 with 60 dBA contours.

It is easy to note that, as shown in Figure 5a, the flight paths related to the minimum noise are remarkably different with respect to the minimum fuel solution. Such solutions are also distant from each other in the objectives space: this is highlighted in Figure 5b, which shows substantial differences between the 60 dBA areas. The minimum noise solution consists of an initial steep climb with a maximum ramp angle compatible with the engine overspeed: the steep climb is followed by a low-ramp path. this is reflected in the 60 dBA area enlargement downstream from the runway (at x = 10 km), compensated by its shortening at x = 34 km. It is interesting to note that the minimum fuel solution 60 dBA contour is similar to that related to the reference takeoff (see Figure 5b), which could prove that the reference flight path is designed to reduce chemical emissions.

To better understand the reasons that lead to the modification of the 60 dBA contour shape, let us observe the procedural variables related to the takeoff optimal solutions, reported in Figure 6.
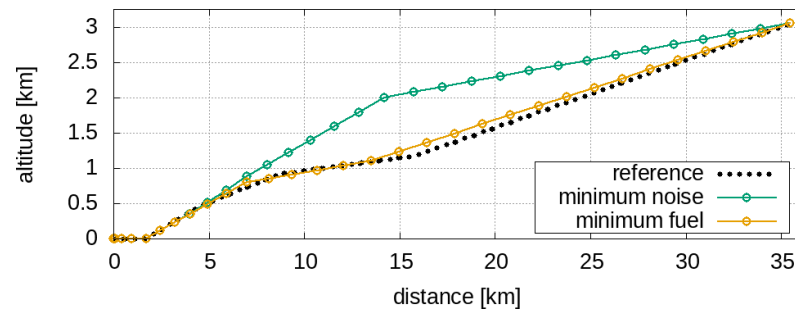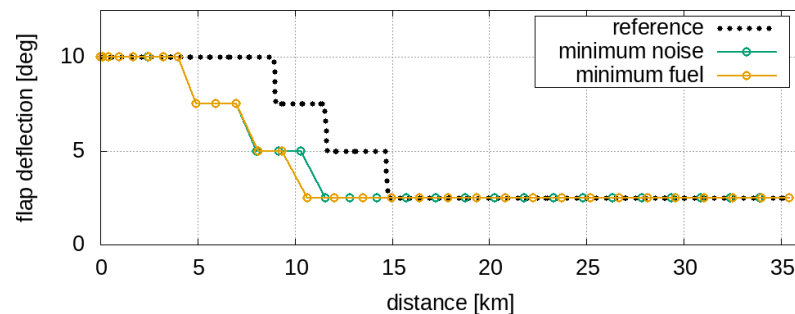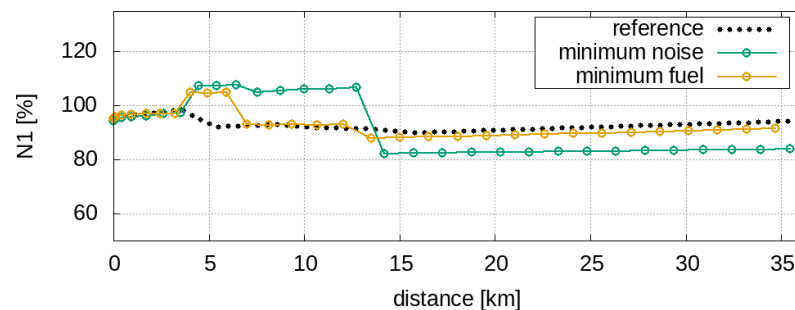
(**a**)
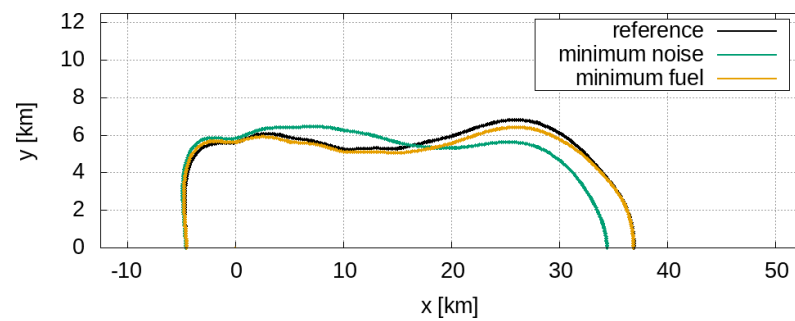
(**b**)

Figure 5. Takeoff manoeuvre for the single-aisle aircraft: flight paths and 60 dBA contours for the reference trajectory and the optimal solutions related to the minimum noise and the minimum fuel consumption: (**a**) flight path, (**b**) 60 dBA contours.

(**a**)

(**b**)

Figure 6. Takeoff manoeuvre for the single-aisle aircraft. Procedural variables. (**a**) flap deflection, (**b**) N1.

Figure 6a shows the time history of the flap deflection: for both optimal solutions, the flap retraction is anticipated, producing less noise with respect to the reference manoeuvre. It is worth noting that, as shown in Figure 6b, the rotational speed N1 for the low-noise

optimal solution exceeds 100%, reaching the overspeed in just under 10 min: this generates more propulsive noise, but the steep climb, as mentioned above, shortens the 60 dBA contour from x = 37 km to x = 34 km at y = 0 km.
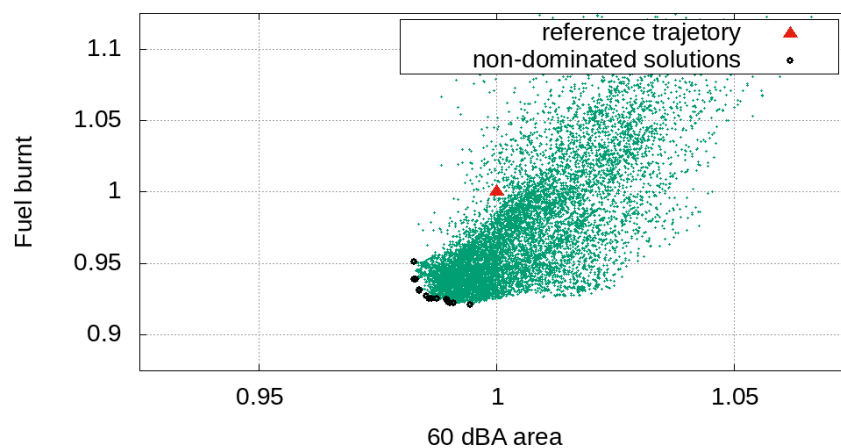
4.1.2. Approach

The second, the third and the fourth trajectory nodes are optimised for the problem related to the approach trajectory: the optimisation variables are reported in Table 5 with the upper and lower bounds.

Table 5. Approach manoeuvre optimisation variables for the single-aisle aircraft: reference values with upper and lower bounds.

Variable	Lower Bound	Reference	Upper Bound
x_2 (m)	−27,500.0	−24,262.8	−22,500.0
z_2 (m)	914.4	914.4	1100.0
v_2 (m/s)	115.0	134.4	140.6
x_3 (m)	−19,000.0	−17,447.8	−16,500.0
z_3 (m)	850.0	914.4	914.4
v_3 (m/s)	95.0	98.0	115.0
x_4 (m)	−15,500.0	−15,202.8	−13,000.0
z_4 (m)	600.0	796.7	850.0
v_4 (m/s)	75.0	539.7	95.0

The DPSO solutions (normalised with respect to the reference solution) for the approach operation related to the single-aisle aircraft are presented in Figure 7 with the approximated Pareto front.
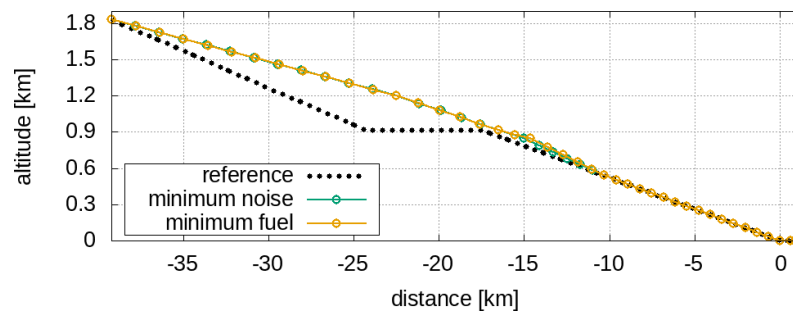

Figure 7. Approach manoeuvre for the single-aisle aircraft: normalised DPSO solutions with reference trajectory and approximated Pareto front.

Figure 7 shows that, also for the approach operation case, as already highlighted for takeoff, the non-dominated solutions are better than the reference solution in terms of both the objective functions. Notwithstanding, in this case the variation of the 60 dBA area is just above 2 km^2 comparing the minimum fuel and the minimum noise optima (which correspond to a relative variation of about 1.5%). In Figure 8, the reference trajectory and the optimal solutions related to the minimum noise and the minimum fuel consumption are presented.

The analysis of Figure 8b shows that the contours of the 60 dBA areas almost overlap, but both are different from the 60 dBA area contour of the reference approach flight path. Indeed, as can be seen in Figure 8a, the minimum noise and the minimum fuel trajectories are almost identical, both tending to the continuous descent approach (CDA) with a −3° slope.

The analysis of the procedural variables related to the approach optimal solutions, reported in Figure 9, also shows that the optimal operations are very similar.
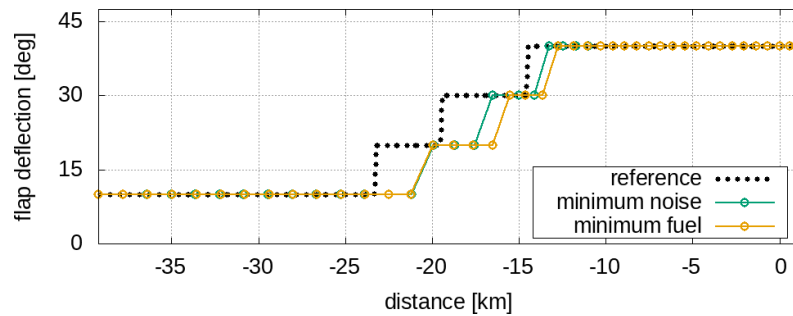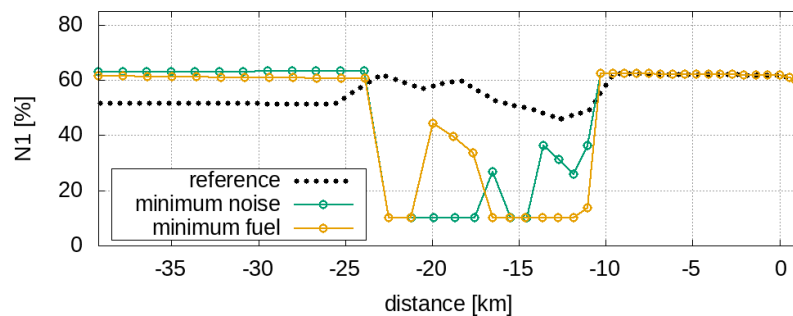

(**a**)
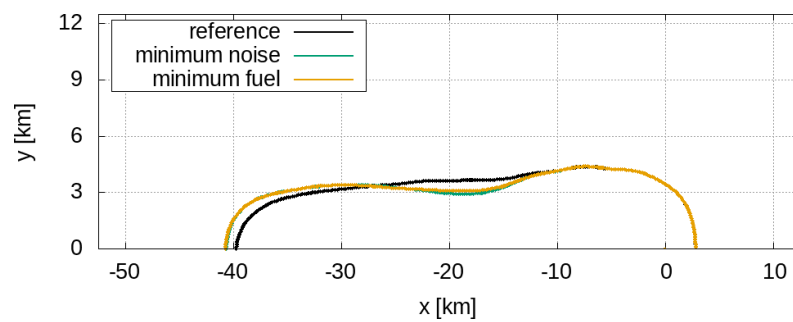
(**b**)

Figure 8. Approach manoeuvre for the single-aisle aircraft: flight paths and 60 dBA contours for the reference trajectory and the optimal solutions related to the minimum noise and the minimum fuel consumption: (**a**) flight path, (**b**) 60 dBA contours.

(**a**)

(**b**)

Figure 9. Approach manoeuvre for the single-aisle aircraft. Procedural variables. (**a**) flap deflection, (**b**) N1.

The flap deployment of both the optimal operations, reported in Figure 9a, is delayed if compared to the reference manoeuvre, whereas N1, shown in Figure 9b, tends to the idle condition in the flight path segment from x = −25 km to x = −10 km. The different engine operating point, combined with a greater altitude, implies a reduction in the 60 dBA contour at x = −20 km related to the optimal solution with respect to the reference one, as depicted in Figure 8b.

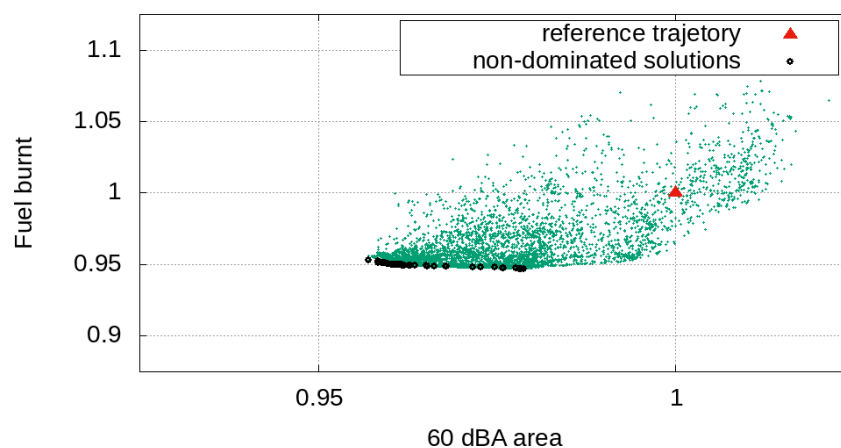### 4.2. Twin-Aisle Aircraft
4.2.1. Takeoff

The takeoff optimisation, as for the single-aisle aircraft, aims at finding the optimal flight path in terms of three nodal variables (the third, the fourth and the fifth trajectory nodes). The design variables with the upper and lower bounds are reported in Table 6 with the upper and lower bounds.

Table 6. Takeoff manoeuvre optimisation variables for the twin-aisle aircraft: reference values with upper and lower bounds.

| Variable	Lower Bound	Reference	Upper Bound
x_3 (m)	4000.0	4772.2	5500.0
z_3 (m)	350.0	457.2	700.0
v_3 (m/s)	87.9	85.6	90.0
x_4 (m)	7000.0	9571.5	11,000.0
z_4 (m)	700.0	914.4	1100.0
v_4 (m/s)	90.0	87.5	115.0
x_5 (m)	13,500.0	16,285.3	20,000.0
z_5 (m)	1100.0	1179.4	2000.0
v_5 (m/s)	115.0	136.2	149.7

The DPSO solutions (normalised with respect to the reference solution) and the approximated Pareto front are depicted in Figure 10 for the takeoff optimisation related to the twin-aisle aircraft.

The non-dominated solutions of Figure 10 show that it is possible to decrease the 60 dBA area by about 10% starting from the minimum fuel solution moving along the Pareto front (as already discussed for the single-aisle takeoff optimisation shown in Figure 4). Once again, the approximated Pareto frontier is composed of solutions that improve both objectives if compared with the reference takeoff flight path. Figure 5 depicts the the optimal solutions related to the minimum noise and the minimum fuel consumption with the 60 dBA contours.
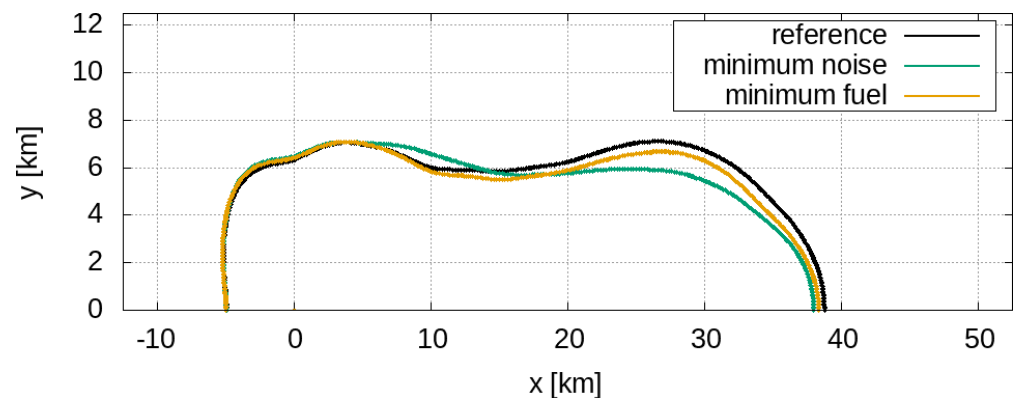

Figure 10. Takeoff manoeuvre for the twin-aisle aircraft: normalised DPSO solutions with reference trajectory and approximated Pareto front.

Figure 11a shows that, as already noted in Figure 5a for the single-aisle aircraft, the minimum fuel solution and the minimum noise one are remarkably different. The behaviour highlighted above for the minimum noise optimal solution is here confirmed: the twin-aisle minimum noise takeoff also corresponds to an initial steep climb followed by a low-ramp flight path. The 60 dBA contour distortion with respect to the reference trajectory is similar to the previous case, but is less evident because the aircraft is larger and the engines need to provide more thrust, causing a more intense propulsive noise. The minimum fuel solution flight path is quite different from the reference trajectory, but their 60 dBA contours (in Figure 5b) manifest many similarities.
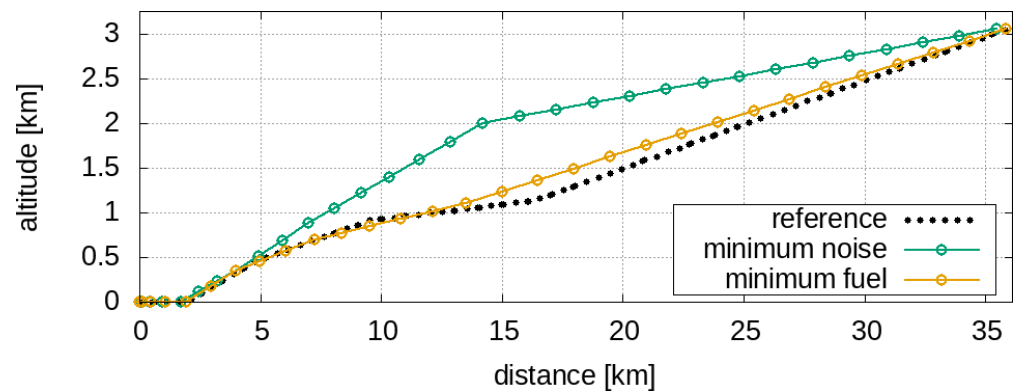

(**a**) Flight paths

(**b**) 60 dBA contours

Figure 11. Takeoff manoeuvre for the twin-aisle aircraft: flight paths and 60 dBA contours for the reference trajectory and the optimal solutions related to the minimum noise and the minimum fuel consumption: (**a**) flight path, (**b**) 60 dBA contours.

As already carried out for the single-aisle aircraft, let us analyse the procedural variables (in terms of flap and N1 time history) related to the takeoff optimal solutions, reported in Figure 12.

Again this time, the flap deployment anticipates both the solutions, as can be observed in Figure 6b, as a result of higher aircraft acceleration. However, as regards N1, only the solution related to the minimum noise is characterised by the engine overspeed in the first phase of the climb, as shown in Figure 6b: instead, the engine operating points related to the minimum fuel solution are comparable to those of the reference solution, as well as the flight path, resulting in a similar 60 dBA contour (see Figure 11b).

(**a**) Flap deflection

(**b**) N1
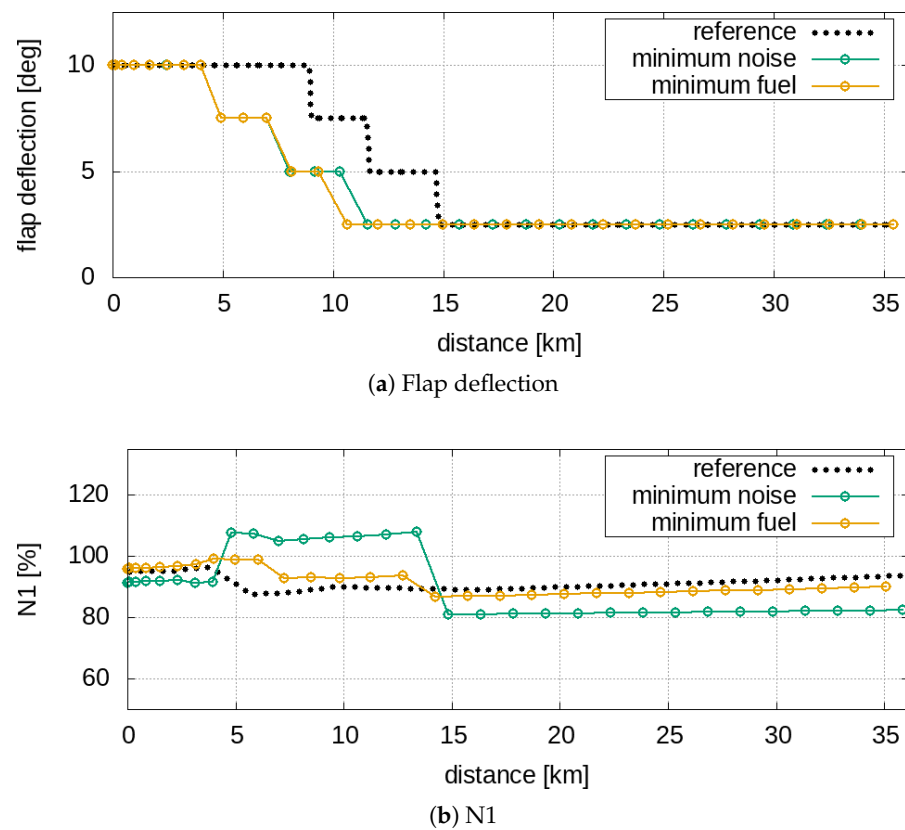
Figure 12. Takeoff manoeuvre for the twin-aisle aircraft. Procedural variables. (**a**) flap deflection, (**b**) N1.
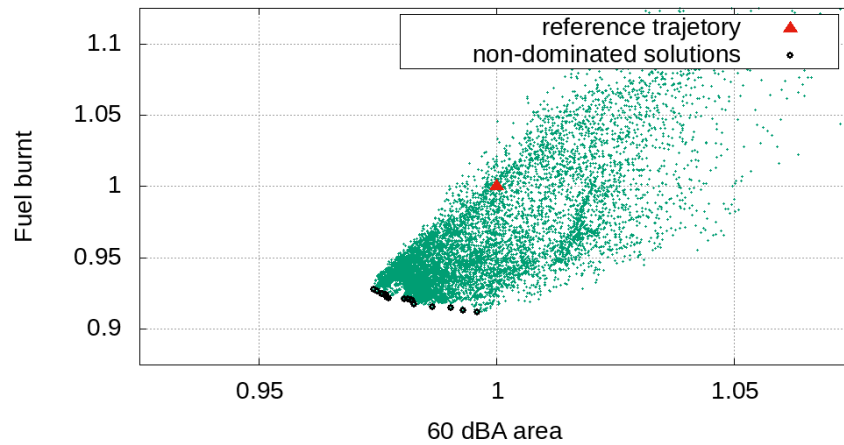
4.2.2. Approach

The optimisation process for the landing is aimed at finding the optimal path in terms of spatial and kinematic variables of three nodes (the second, the third and the fourth trajectory nodes): the optimisation variables, with the upper and lower bounds, are reported in Table 7.

Table 7. Approach manoeuvre optimisation variables for the twin-aisle aircraft: reference values with upper and lower bounds.

Variable	Lower Bound	Reference	Upper Bound
x_2 (m)	−30,000.0	−24,262.8	−22,500.0
z_2 (m)	914.4	914.4	1200.0
v_2 (m/s)	115.0	134.4	140.6
x_3 (m)	−20,000.0	−17,447.8	−16,500.0
z_3 (m)	845.0	914.4	914.4
v_3 (m/s)	85.0	89.3	115.0
x_4 (m)	−15,500.0	−14,813.2	−13,500.0
z_4 (m)	637.5	796.7	845.0
v_4 (m/s)	69.4	82.3	85.0

Figure 13 presents the DPSO solutions (normalised with respect to the reference solution) with the reference trajectory and the approximated Pareto front related to the approach operation optimisation for the twin-aisle aircraft.
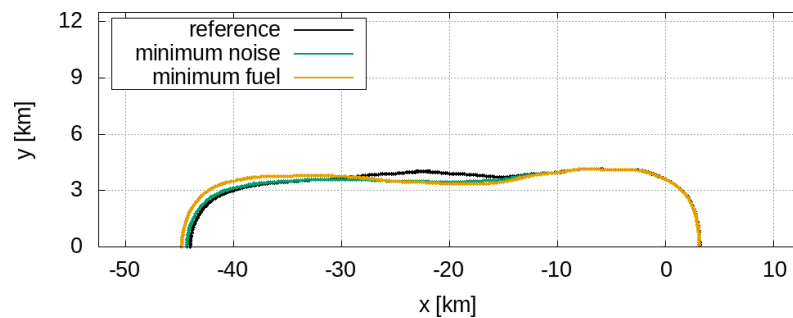
Figure 13. Approach manoeuvre for the twin-aisle aircraft: normalised DPSO solutions with reference trajectory and approximated Pareto front.

All the non-dominated solutions of Figure 13 improve the reference solution in terms of both the noise emission and the fuel consumption (as already noted for the cases of Figures 4, 7 and 10). The 60 dBA area relative variation of the minimum noise solution with respect to the minimum fuel one is 2%, corresponding to about 7 km^2. In Figure 14 are depicted the optimal solutions related to the minimum noise and the minimum fuel consumption with the reference trajectory.
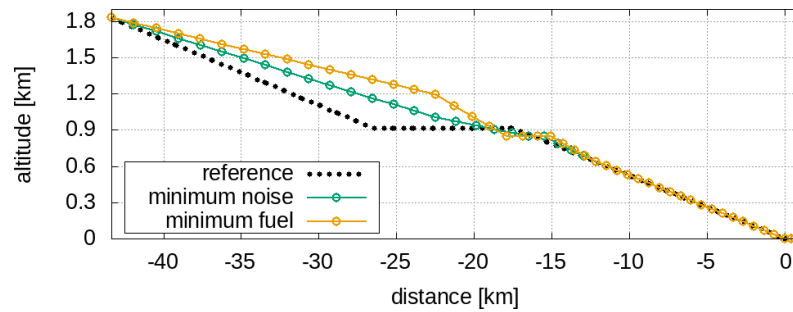
(**a**)

(**b**)

Figure 14. Approach manoeuvre for the twin-aisle aircraft: flight paths and 60 dBA contours for the reference trajectory and the optimal solutions related to the minimum noise and the minimum fuel consumption: (**a**) flight path, (**b**) 60 dBA contours.

Despite the similar 60 dBA areas, Figure 14b shows that the contours related to the minimum noise and the minimum fuel solutions do not overlap with that related to the reference trajectory, especially at x = −45 km and x = −20 km. In fact, the two analysed optimal solutions correspond to two rather different paths: the minimum noise trajectory tends to the CDA (as for the single-aisle case of Figure 8a), whereas the minimum fuel path

shows two different slope angles up to x = −18 km and preserves a zero-slope path for 18 < x < −15 km.

Figure 15 shows the procedural variables related to the approach's optimal solutions for the approach's optimal operations.
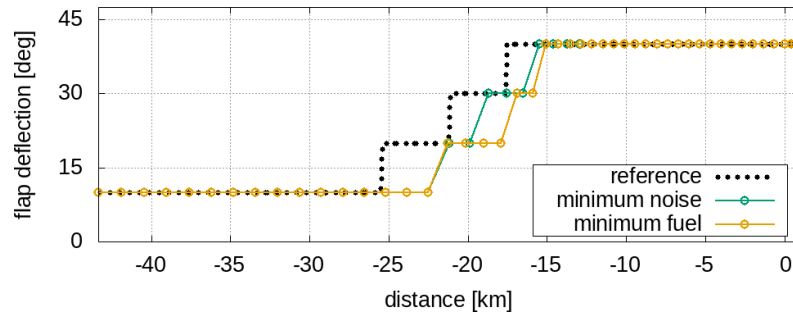
(**a**)
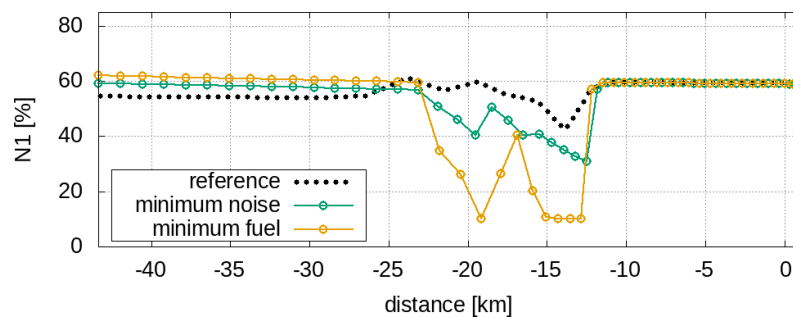
(**b**)

Figure 15. Approach manoeuvre for the twin-aisle aircraft. Procedural variables. (**a**) flap deflection, (**b**) N1.

The same considerations made for the single-aisle aircraft are valid in this case. A flap deployment delay can be observed (see Figure 15b) in both the minimum noise and the minimum fuel solution with respect to the reference one. The engine operating points from x = −25 km to x = −10 km are lower than the reference procedure, as depicted in Figure 15b, and this behaviour justifies the reduction of the 60 dBA contour (see Figure 14b) together with the greater aircraft altitude.

5. Sound-Quality-Based Decision Making

It is known that the single-objective optimisation problem leads to the identification of a unique design space point corresponding to the minimum of the objective function, which can be considered by the designer as the optimal solution. In contrast, the multiobjective problem solution consists of a set of non-dominated optimal solutions that constitute the Pareto frontier; therefore, from the designer's point of view the choice of the optimum among the Pareto front plays a key role. It is worth noting that the Pareto front could be a mathematically consistent but technically irrelevant entity, and this occur when the non-dominated solutions are close to each other both in the domain and in the codomain: in this case, the designer can consider the whole set of optimal solutions as a unique optimum. On the other hand, when the solutions are far both in the domain and in the codomain (or even close in the domain and far away in the codomain), the need to establish a criterion for decision making has a paramount relevance.

In the view of sustainable airport scenarios, a viable strategy is including the quality of the noise within the decision making process: this can be done by comparing the noise produced by the aircraft and a weakly annoying target sound. Such an approach is based on the measure of the matching of the noise emitted by the operation under analysis with a

previously defined weakly annoying sound. The noise reaching the virtual microphone during a flight operation is characterised by a specific spectrogram, which provides the amplitude of the noise event in the time-frequency domain. Thus, let us consider the vector space defined by the difference between the spectrogram S_c related to the current flight path and the spectrogram S_t related to the target sound

$$\Delta = S_c(f,t) - S_t(f,t) \tag{11}$$

The norm of Δ in the L^p space can be used as a metric to quantify the similarity of the actual spectrogram with respect to the target one. Accordingly, the sound-matching index $\mathcal{I}_{SM}$ can be formalised as follows

$$\mathcal{I}_{SM}^p = ||\Delta||_p = \left[\frac{1}{T} \frac{1}{F} \int_{t_1}^{t_2} \int_{f_{min}}^{f_{max}} |S_c(f,t) - S_t(f,t)|^p df dt \right]^{\frac{1}{p}} \tag{12}$$

where $T = t_2 - t_1$ and $F = f_{max} - f_{min}$. The target sounds used in this work were synthesised on the basis of psychometric test campaigns performed within the projects SEFA and COSMA [14,17]. It is worth noting that the choice of p can be exploited by the designer to focus the metric on tonal broadband or tonal component dissimilarities (low and high values of p, respectively); indeed, low values of p enhance the contribution of distributed differences and high values of p emphasise the local ones. Optimisation problems involving $\mathcal{I}_{SM}$ have been successfully used in both the aircraft conceptual design and single-point low-noise flight path optimisation [16,22].

Figure 16 shows a pictorial representation of the sound-matching concept, and depicts the spectral comparison of two signals (solution A and B) with respect to a target spectrum for a certain time instant.
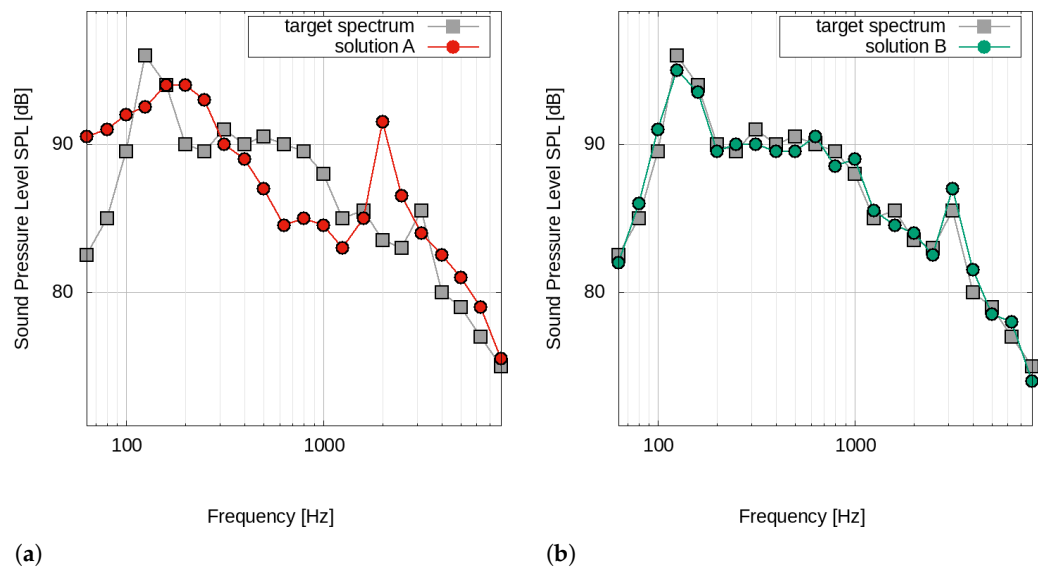
Figure 16. Example of spectral matching. (**a**) solution A: poor matching. (**b**) solution B: good matching.

The spectral properties related to solution A of Figure 16a are quite different with respect to the target spectrum: in this case, Equation (12) (in this example with $p = 2$) returns a high value of $\mathcal{I}_{SM}$. In contrast, solution B (see Figure 16b) turns out to have frequency characteristics similar to the target spectrum; therefore, the $\mathcal{I}_{SM}$ value is low. In the case of an entire manoeuvre simulation, the $\mathcal{I}_{SM}$ value is simply a cumulative value over all the analysed time instants.

Pareto Solution Analysis and Designer's Choice

Let us consider the optimisation results reported in Section 4. Figures 5a and 11a (single- and twin-aisle takeoff operations) show the solutions related to the different minimum noise and minimum fuel produce trajectories in terms of geometric, kinematic and procedural variables; even in the codomain, the two solutions turn out to be distant from each other as the contours of the 60 dBA areas have different shapes (see Figures 5b and 11b). The minimum noise and the minimum fuel approach operations of the twin-aisle aircraft depicted in Figure 14a are quite different paths, but Figure 14b shows that there are no relevant discrepancies between the 60 dBA contours (both different form the reference flight path). As said, this also applies to the 60 dBA contours related to the single-aisle aircraft solutions (in Figure 8b); in this case, the similarity between the noise footprints is justified by two practically identical trajectories, depicted in Figure 8a.

It must be noted that the behaviour of the solutions for the approach manoeuvres (in Figures 8 and 14) is not surprising since the entire last part of the flight path is constrained by strict regulations that impose a $-3°$ ramp angle. For the sound quality assessment, let us consider a virtual microphone placed under the flight path at x = -7.5 km (see Figures 8 and 14) that represents an urbanised location close to the airport boundary; it should be expected that there are no large variations in the time-frequency contributions of noise in landing operations, and this is confirmed by Figure 17, which depicts the mapped approximated Pareto optimal solutions with the sound-matching index $\mathcal{I}_{SM}$ as a parameter for the approach operations.

(**a**)   (**b**)
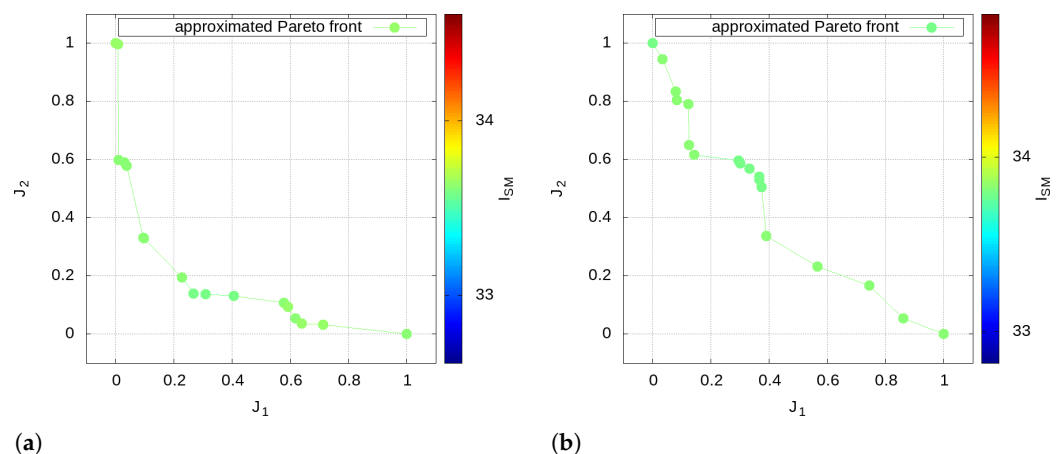
Figure 17. Solutions of the multiobjective problems for the approach operations: mapped approximated Pareto optimal solutions with the sound-matching index $\mathcal{I}_{SM}$ as parameter. The solutions with the minimum $\mathcal{I}_{SM}$ cannot be found. (**a**) single–aisle, (**b**) twin–aisle.

The designer should therefore choose the trajectory related to the lowest fuel consumption, as each Pareto solution, despite being better than the reference one, is very similar to the others in terms of noise footprint and spectral components

Regarding the takeoff operations, the choice of the optimal solution among the Pareto front is addressed by means of the sound-matching index $\mathcal{I}_{SM}$ using $p = 2$ (see Equation (12)). Let us consider a virtual microphone close to the airport boundary x = 4.5 km; Figure 18 shows the mapped approximated Pareto optimal solutions with the sound-matching index $\mathcal{I}_{SM}$ as parameter related to the takeoff operation for both the single- and the twin-aisle aircraft.

(a)   **(b)**
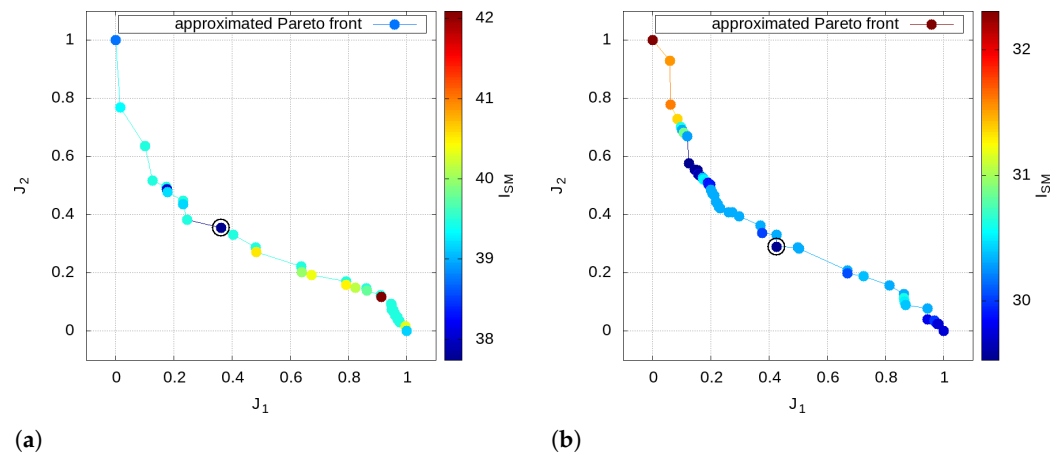
Figure 18. Solutions of the multiobjective problems for the takeoff operations: mapped approximated Pareto optimal solutions with the sound-matching index $\mathcal{I}_{SM}$ as parameter. The marked solutions are the ones with the minimum $\mathcal{I}_{SM}$. (**a**) single–aisle, (**b**) twin–aisle.

The analysis of Figure 18 highlights that there is not a specific functional dependency between the 60 dBA contour, the fuel consumption and the spectral content of the noise: indeed, the distribution of $\mathcal{I}_{SM}$ turns out to be in apparently random locations along the Pareto front. It is worth noting that the great variability of the $\mathcal{I}_{SM}$ demonstrates how this approach guarantees the designer an additional degree of freedom in the takeoff optimisation; this could be explained by considering the great sensitivity of the noise tonal components with respect to the variations in the engine operating point during the takeoff operations.

6. Conclusions

Nowadays, the introduction of alternative paradigms in the management of airport noise is becoming an imperative need. This work presents a multiobjective optimisation of takeoff and approach concerning low-noise procedures of single- and twin-aisle commercial aircraft with special attention paid to the sound-quality assessment of the MOP solutions. To simultaneously mitigate both the acoustic and chemical emissions, two merit functions are minimised through a multiobjective and multidisciplinary optimisation problem. The first objective function is the SEL 60 dBA contour area, and the amount of fuel burn is used as the second objective. The optimisation problems are carried out within the in-house MCRDO framework FRIDA. The results related to the approach operations show that, due to the strict regulations that impose a $-3°$ ramp angle during the last phase of the manoeuvre, the 60 dBA contour can only be minimally decreased; thus, the designer's choice can fall on the solution related to minimum fuel consumption. The takeoff problems show a large margin of choice among the Pareto solutions, which is why an additional objective function to select the final configuration must be introduced. The latter is defined as the norm of the difference between the noise produced by the configuration under analysis and a weakly annoying target sound, and the designer is free to choose the solution corresponding to the best sound quality. The results demonstrate that the sound-quality assessment can successfully help the designer to select the optimal flight path by providing an additional degree of freedom within the optimisation loop.

Author Contributions: Conceptualisation, U.I. and F.C.; methodology, U.I. and F.C.; software, F.C.; validation, F.C.; formal analysis, U.I. and F.C.; investigation, F.C.; writing, original draft preparation, F.C.; writing, review and editing, U.I. and F.C.; supervision, U.I.; project administration, U.I.; funding acquisition, U.I. All authors have read and agreed to the published version of the manuscript.

Institutional Review Board Statement: Not applicable.

Informed Consent Statement: Not applicable.

**Conflicts of Interest:** The authors declare no conflict of interest.

Abbreviations

The following abbreviations are used in this manuscript:

ANIMA	Aviation Noise Impact Management through Novel Approaches
BWB	Blended Wing Body
CDA	Continuous Descent Approach
COSMA	Community Noise Solutions to Minimise aircraft noise Annoyance
DPSO	Deterministic PSO
FAA	Federal Aviation Administration
FRIDA	Framework for Innovative Design in Aeronautics
ICAO	International Civil Aviation Organization
MOP	Multiobjective Optimisation Problem
MCRDO	Multidisciplinary Conceptual Robust Design Optimisation
MTOW	Maximum Takeoff Weight
NAP	Noise Abatement Procedure
OEW	Operating Empty Weight
PSO	Particle Swarm Optimisation
SEFA	Sound EngineeringFor Aircraft
SEL	Sound Exposure Level
TAS	True Air Speed
UAM	Urban Air Mobility

Appendix A. FRIDA

The tool FRIDA (Framework for Innovative Design in Aeronautics) is the Multidisciplinary Conceptual Robust Design Optimisation (MCRDO) framework developed by the Aerospace Structures and Design group of the Roma Tre University. The framework is characterised by a collection of simulation modules and a library of optimisation methods that can be called in the appropriate sequence to execute direct simulations, optimisation, quantification of uncertainties, design-space exploration, surrogate modelling or any combination these fundamental tasks (see Figure A1 and Knobloch et al. [1] for details).
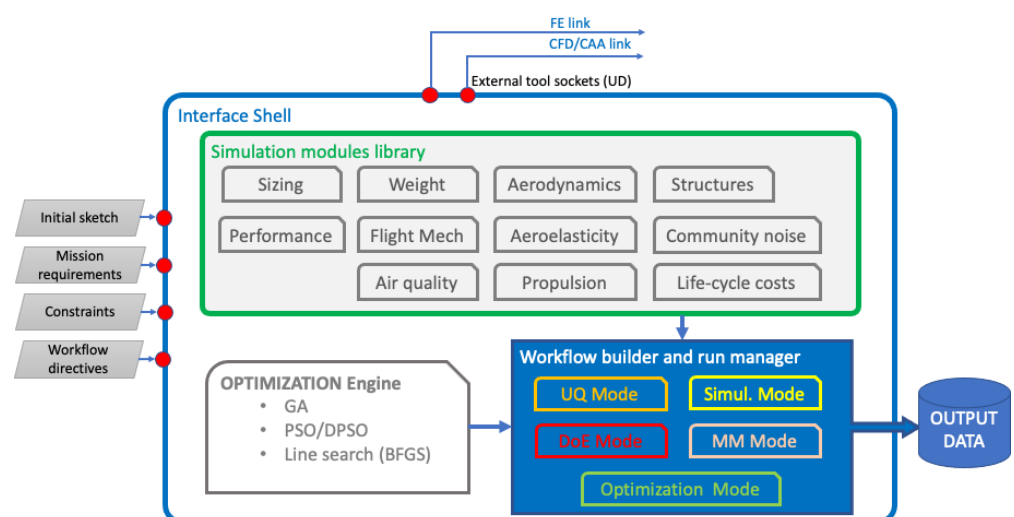
Figure A1. Conceptual layout of the FRIDA tool.

The specific workflow needed to attain a particular objective can be easily built taking advantage of the structure of the tool. Figure A2 depicts the block diagram of the workflow adopted for the optimisation of procedures presented in this work. It is worth noting how the constraints due to regulation (highlighted in yellow in Figure A2) strongly influence

the variance of the non-dominated set. Indeed, the limitations imposed for the approach procedures restrict the maximum variation of the Pareto solutions to less than 10 kg of fuel and 10 km^2 of $|A_{60}|$.

The estimate of the engine noise sources and the fuel consumption requires the knowledge of the engine operating points at each trajectory sample. With this aim, a semi-empirical turbofan model was implemented. For a prescribed flight condition, the model provides the percentage of throttle, t$_\%$, as a function of the flight mechanics variable $\mathbf{X}_{fm}$ (altitude, drag force, actual aircraft weight, acceleration of the aircraft, etc.) and the engine characteristics $\mathbf{X}_{eng}$ (engine pitch, bypass ratio, maximum thrust at sea level, etc.).
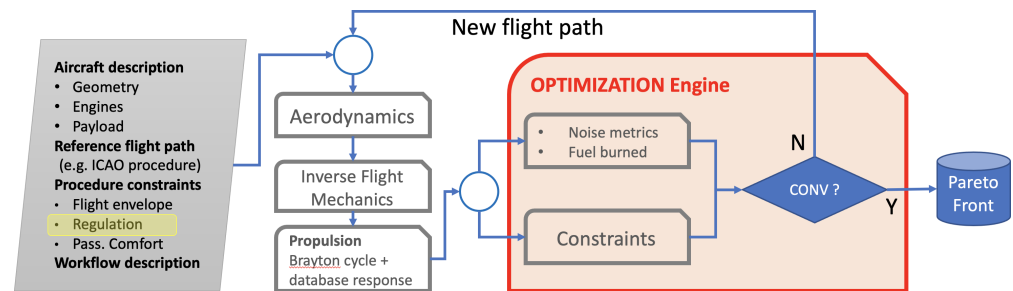

Figure A2. FRIDA workflow for the procedure optimisation.

Starting from the throttle percentage, the rotational speeds $N1$ and $N2$ of low-pressure and high-pressure spools, respectively, are evaluated. The jet velocities are then calculated through the momentum equation and their temperatures are estimated with the energy balance. The airframe and the engine noise are estimated within the aeroacoustics module. The noise of lifting surfaces, tail, high-lift devices and landing gears is based on semi-empirical functions according to Fink's model [26,27]. The engine noise estimate is based on the Morfey and Fisher model [28,29] for the buzz-saw noise and Heidmann's model [30] for the fan and the compressor noise. The jet noise is calculated by means of an interpolating metamodel built from available data. The calculation of the one-third octave band Sound Pressure Level (SPL) takes into account the Doppler effect, the atmospheric absorption [31] and the ground reflection. The Sound Exposure Level (SEL) and the Effective Perceived Noise Level (EPNL) are also estimated by means of a suitable postprocessing. More recently, surrogate models of the engine noise shielding effects for unconventional configurations (like, e.g., the Blended Wing Body) have been implemented. A financial module, which allows the estimation of financial implications from an airline company perspective [20], is also included in FRIDA. The positive cash flows (related to revenues) and the negative ones (fuel and maintenance costs, and social costs related to noise pollution) are calculated and actualised to evaluate the airliner net present value.

References

1. Knobloch, K.; Manoha, E.; Atinault, O.; Barrier, R.; Polacsek, C.; Lorteau, M.; Iemma, U.; Centracchio, F.; Rossetti, M.; Cioffi, I.; et al. Future Aircraft and the Future of Aircraft Noise. In *Aviation Noise Impact Management: Technologies, Regulations, and Societal Well-Being in Europe*; Leylekian, L., Covrig, A., Maximova, A., Eds.; Springer International Publishing: Cham, Switzerland, 2022; pp. 117–139. [CrossRef]
2. Dancila, R.; Botez, R. New flight trajectory optimisation method using genetic algorithms. *Aeronaut. J.* **2021**, *125*, 618–671. [CrossRef]
3. Gardi, A.; Sabatini, R.; Ramasamy, S. Multi-objective optimisation of aircraft flight trajectories in the ATM and avionics context. *Prog. Aerosp. Sci.* **2016**, *83*, 1–36. [CrossRef]
4. Zhang, M.; Filippone, A.; Bojdo, N. Multi-objective optimisation of aircraft departure trajectories. *Aerosp. Sci. Technol.* **2018**, *79*, 37–47. [CrossRef]
5. Prats, X.; Puig, V.; Quevedo, J. A multi-objective optimization strategy for designing aircraft noise abatement procedures. Case study at Girona airport. *Transp. Res. Part Transp. Environ.* **2011**, *16*, 31–41. [CrossRef]
6. Behere, A.; Mavris, D.N. Optimization of Takeoff Departure Procedures for Airport Noise Mitigation. *Transp. Res. Rec.* **2021**, *2675*, 81–92. [CrossRef]

7. Khardi, S.; Abdallah, L. Optimization approaches of aircraft flight path reducing noise: Comparison of modeling methods. *Appl. Acoust.* **2012**, *73*, 291–301. [CrossRef]

8. Camilleri, W.; Chircop, K.; Zammit-Mangion, D.; Sabatini, R.; Sethi, V. Design and Validation of a Detailed Aircraft Performance Model for Trajectory Optimisation. In Proceedings of the AIAA Modeling and Simulation Technologies Conference, Minneapolis, MN, USA, 13–16 August 2012. [CrossRef]

9. Dancila, B.D.; Botez, R.; Labour, D. Fuel burn prediction algorithm for cruise, constant speed and level flight segments. *Aeronaut. J.* **2013**, *117*, 491–504. [CrossRef]

10. Delfs, J.; Bertsch, L.; Zellmann, C.; Rossian, L.; Kian Far, E.; Ring, T.; Langer, S.C. Aircraft Noise Assessment—From Single Components to Large Scenarios. *Energies* **2018**, *11*, 429. [CrossRef]

11. Elango, P.; Mohan, R. Trajectory optimisation of six degree of freedom aircraft using differential flatness. *Aeronaut. J.* **2018**, *122*, 1788–1810. [CrossRef]

12. Centracchio, F.; Rossetti, M.; Iemma, U. Approach to the Weight Estimation in the Conceptual Design of Hybrid-Electric-Powered Unconventional Regional Aircraft. *J. Adv. Transp.* **2018**, *2018*. [CrossRef]

13. Burghignoli, L.; Rossetti, M.; Centracchio, F.; Palma, G.; Iemma, U. Adaptive RBF with hyperparameter optimisation for aeroacoustic applications. *Int. J. Aeroacoust.* **2022**, *21*, 22–42. [CrossRef]

14. European Commission. SEFA: Sound Engineering for Aircraft. Community Research and Development Information Service, from 1 February 2004 to 30 June 2007. Available online: https://cordis.europa.eu/project/id/502865/reporting/fr (accessed on 25 February 2022).

15. Diez, M.; Iemma, U.; Marchese, V. A sound-matching-based approach for aircraft noise annoyance alleviation via MDO. In Proceedings of the 13th AIAA/CEAS Aeroacoustics Conference, Rome, Italy, 21–23 May 2007.

16. Diez, M.; Iemma, U. Multidisciplinary conceptual design optimization of aircraft using a sound–matching-based objective function. *Eng. Optim.* **2012**, *44*, 591–612. [CrossRef]

17. European Commission. COSMA: Community Oriented Solutions to Minimise Aircraft Noise Annoyance. Community Research and Development Information Service, from 1 June 2009 to 31 March 2013. Available online: https://trimis.ec.europa.eu/project/community-oriented-solutions-minimise-aircraft-noise-annoyance (accessed on 25 February 2022).

18. Iemma, U. Multi-disciplinary, community-oriented design of low-noise aircraft: The COSMA project. *Noise Mapp.* **2016**, *3*, 59–70. [CrossRef]

19. European Commission. ANIMA: Aviation Noise Impact Management through Novel Approaches. Community Research and Development Information Service, from 1 October 2017 to 31 December 2021. Available online: https://cordis.europa.eu/project/id/769627 (accessed on 25 February 2022).

20. Iemma, U.; Pisi Vitagliano, F.; Centracchio, F. A multi-objective design optimisation of eco-friendly aircraft: The impact of noise fees on airplanes sustainable development. *Int. J. Sustain. Eng.* **2017**, *11*, 122–134. [CrossRef]

21. Bernardini, G.; Centracchio, F.; Gennaretti, M.; Iemma, U.; Pasquali, C.; Poggi, C.; Rossetti, M.; Serafini, J. Numerical Characterisation of the Aeroacoustic Signature of Propeller Arrays for Distributed Electric Propulsion. *Appl. Sci.* **2020**, *10*, 2643. [CrossRef]

22. Centracchio, F.; Burghignoli, L.; Iemma, U. Multiobjective optimisation of flight paths for noise level mitigation and sound quality improvement. *Noise Mapp.* **2021**, *8*, 268–280. [CrossRef]

23. Kennedy, J. Particle swarm optimization. In Proceedings of the 1995 IEEE International Conference on Neural Networks, Perth, Australia, 27 November–1 December 1995; Volume 4, pp. 1942–1948. [CrossRef]

24. Campana, E.; Diez, M.; Fasano, G.; Peri, D. Initial particles position for PSO, in Bound Constrained Optimization. In *Advances in Swarm Intelligence*; Lecture Notes in Computer Science; Tan, Y., Shi, Y., Mo, H., Eds.; Springer: Berlin/Heidelberg, Germany, 2013; Volume 7928, pp. 112–119.

25. Pellegrini, R.; Serani, A.; Leotardi, C.; Iemma, U.; Campana, E.F.; Diez, M. Formulation and parameter selection of multi-objective deterministic particle swarm for simulation-based optimization. *Appl. Soft Comput.* **2017**, *58*, 714–731. [CrossRef]

26. Fink, M.R. Approximate prediction of airframe noise. *J. Aircr.* **1976**, *13*, 833–834. [CrossRef]

27. Fink, M.R. Airframe noise prediction. In *Federal Aviation Administration Report FAA–RD–77–29*; Federal Aviation Administration: Washington, DC, USA, 1977.

28. Morfey, C.; Fisher, M. Shock–Wave radiation from a supersonic ducted rotor. *Aeronaut. J.* **1970**, *74*, 579–585.

29. McAlpine, A.; Fisher, M. On the prediction of buzz–saw noise generated by an aero–engine. In Proceedings of the 6th Aeroacoustics Conference and Exhibit, Lahaina, HI, USA, 12–14 June 2000.

30. Heidmann, M. *Interim Prediction Method for Fan and Compressor Source Noise*; NASA TM-X-71763; NASA: Washington, DC, USA, 1979.

31. Sutherland, L.; Piercy, J. Method for calculating the absorption of sound by the atmosphere. In Proceedings of the 88th Meeting of the Acoustical Society of America, Washington, DC, USA, 22–24 April 1974.